How to cite: *Angew. Chem. Int. Ed.* **2021**, *60*, 17564–17569
International Edition: doi.org/10.1002/anie.202103486
German Edition: doi.org/10.1002/ange.202103486

Photonic Materials

Facet Selectivity Guided Assembly of Nanoarchitectures onto Two-Dimensional Metal–Organic Framework Nanosheets

*Zhihao Li[+], Huajian Gao[+], Ruichen Shen[+], Caixin Zhang, Leisi Li, Yawei Lv, Liming Tang, Yaping Du, and Quan Yuan**

Abstract: *Facet-selective nanostructures in living systems usually exhibit outstanding optical and enzymatic properties, playing important roles in photonics, matter exchange, and biocatalysis. Bioinspired construction of facet-selective nanostructures offers great opportunities for sophisticated nanomaterials, but remains a formidable task. We have developed a macromolecule-mediated strategy for the assembly of upconversion nanoparticles (UCNPs)/two-dimensional metal–organic frameworks (2DMOFs) heterostructures with facet selectivity. Both experimental and theoretical results demonstrate that polyvinylpyrrolidone (PVP) can be utilized as an interface-selective mediator to further promote the facet-selective assembly of MOFs onto the surface of UCNPs. The UCNPs/2DMOFs nanostructures with facet selectivity display specific optical properties and show great advantages in anti-counterfeiting. Our demonstration of UCNPs/2DMOFs provides a vivid example for the controlled fabrication of facet-selective nanostructures and can promote the development of advanced functional materials for applications in biosensing, energy conversion, and information assurance.*

Introduction

In nature, almost all living organisms can delicately regulate the growth and assembly of inorganic crystals under the direction of macromolecules.[1] These biologically controlled processes have created enormous hierarchical nanostructures and played important roles in biological functions such as photonics,[2] mechanical support,[3] matter exchange,[4] and energy transfer.[5] Generally, such well-defined functions usually result from the sophisticated anisotropy and fascinating morphology of assembled nanostructures, especially the surface-related physical and chemical properties.[6] Of particular interest, as one of the most important surface properties, the crystal facet has recently aroused intensive attention in the assembly of biomineralized nanostructures.[7] For example, it has been widely investigated that facet properties of inorganic crystals play significant roles during the process of bone formation.[7b,8] Specifically, owing to the facet-selective interaction between proteins and inorganic crystals, the orientation and polymorph of bone nanostructures are delicately regulated with outstanding mechanical functions.[8,9] Except for that, nanostructures assembled with facet selectivity have also been demonstrated to display fantastic facet-dependent optical properties and enzymatic properties, enabling huge advantages in fields including photonics,[10] metabolism,[11] and catalysis.[12] Therefore, bioinspired construction of facet-selective nanostructures can not only help to reveal the growth mechanisms of biominerals with a better understanding of the structure-function relationship, but also offer extensive opportunities for the design and applications of multifunctional advanced materials.

During the assembly of facet-selective biominerals, the interactions between macromolecules and inorganic matrixes play a central role in the control of nucleation, growth, shapes, and geometrical morphology.[13] Macromolecules possess rich functional groups and can serve as binding sites to deposit crystal-forming ions, further promoting the nucleation and growth of assembled nanostructures.[13c,14] More importantly, since the different facets of crystals exhibit different binding energy, macromolecules can also preferentially adsorb into the specific facet with high selectivity, thus directing the facet-selective assembly of complex nanostructures.[13a,15] In this regard, rational design of the selective interaction between

[*] Z. Li,[+] H. Gao,[+] L. Li, Prof. Q. Yuan
Key Laboratory of Biomedical Polymers of Ministry of Education
College of Chemistry and Molecular Sciences
School of Microelectronics, Wuhan University
Wuhan 430072 (China)
E-mail: yuanquan@whu.edu.cn
R. C. Shen,[+] Prof. Q. Yuan
Institute of Chemical Biology and Nanomedicine
State Key Laboratory of Chemo/Biosensing and Chemometrics
College of Chemistry and Chemical Engineering
Hunan University
Changsha 410082 (China)
C. Zhang, Y. Lv, Prof. L. Tang
Department of Applied Physics, School of Physics and Electronics
Hunan University
Changsha 410082 (China)
Prof. Y. P. Du
School of Materials Science and Engineering & National Institute for Advanced Materials, Key Laboratory of Advanced Energy Materials Chemistry, Tianjin Key Lab for Rare Earth Materials and Applications
Centre for Rare Earth and Inorganic Functional Materials
Nankai University
Tianjin 300350 (China)
[+] These authors contributed equally to this work.
Supporting information and the ORCID identification number(s) for the author(s) of this article can be found under: https://doi.org/10.1002/anie.202103486.

macromolecules and inorganic matrixes would provide a highly promising strategy for the construction of facet-selective nanostructures.

In this work, with the assistance of macromolecules, anisotropic upconversion nanoparticles (UCNPs) were assembled with two-dimensional metal–organic frameworks (2DMOFs) nanosheets to construct facet-selective nanostructures. Both experimental results and theoretical calculations indicate that polyvinylpyrrolidone (PVP) can serve as a modulator molecule to preferentially interact with the (100) facet of UCNPs and further promote the facet-selective assembly of UCNPs/2DMOFs heterostructures. Consequently, the assembled nanostructures with selective geometry exhibit specific optical properties owing to the interaction-dependent energy transfer, displaying excellent advantages in information coding. The strategy for the rational design of facet-selective nanostructures offers a powerful tool to regulate the surface properties of nanostructures including chemical composition, surface atoms density, electronic structures, and energy transfer, which may advance the development of more sophisticated nanomaterials for potentials in biosensing, information encryption, and energy conversion.

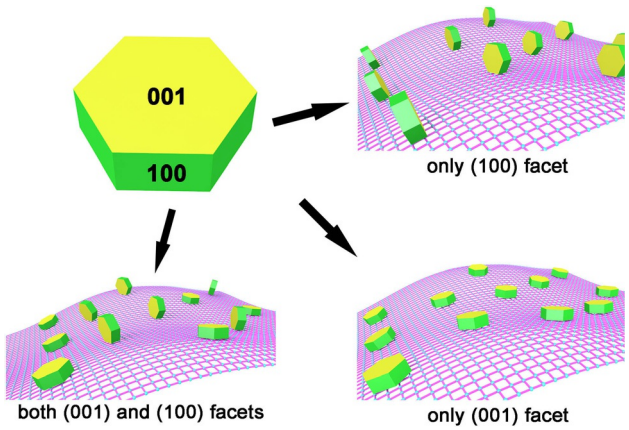

Scheme 1. Three possibilities for 2DMOFs to assemble onto the surface of anisotropic hexagonal UCNPs, including assembling only onto the (100) or (001) facets, and assembling onto both the (100) and (001) facets of UCNPs.

Results and Discussion

2DMOFs exhibit unique properties including ordered micropore structures, ultrathin thickness, large extended dimensions, huge surface area, and numerous active sites.[16] Such properties enable rapid molecular diffusion and efficient mass transfer on the surface of 2DMOFs, guaranteeing the important applications in gas adsorption, catalysis, and biosensing.[16d,e,17] UCNPs, a kind of nanomaterials that can convert NIR light into visible and UV light, exhibits enormous advantages including deep tissue penetration, low background fluorescence, and robust light-harvesting capability.[18] Benefiting from these advantages, UCNPs have found extensive potentials in bioimaging, disease treatment, anticounterfeiting, and energy conversion.[19] Assembly of UCNPs with 2DMOFs can organically integrate the properties of such two materials, promoting the opportunities in catalysis, biomedicine, and information technology. Given the anisotropic structure of UCNPs, assembly of 2DMOFs onto different facets of UCNPs may contribute to diverse optical properties and greatly affect the performance of the nanocomposites. Generally, the most commonly hexagonal UCNPs have two important exposed facets of (001) and (100).[20] Among them, (001) corresponds to top hexagonal surfaces and (100) corresponds to the six lateral rectangular surfaces. In this condition, there are three possibilities for 2DMOFs to assembly onto the surface of UCNPs, including assembling only onto the (100) facet, assembling only onto the (001) facet, and assembling onto both the (100) facet and the (001) facet (Scheme 1).

To investigate the assembly of UCNPs/2DMOFs heterostructures, anisotropic hexagonal UCNPs were firstly synthesized according to a previously reported method.[21] Transmission electron microscopy (TEM) images indicate that as-synthesized UCNPs exhibit a uniform shape of a regular hexagon with a diameter of 90 nm and a height of 60 nm (Figure 1 a; Supporting Information, Figures S1 and S2). Further, UCNPs were functionalized with PVP which can promote the nucleation and assembly of 2DMOFs onto UCNPs. Fourier transform infrared (FTIR) spectroscopy (Figure S3) were used to characterize the groups of oleic acid-capped UCNPs, bare UCNPs and PVP-coated UCNPs. Also, thermogravimetric analysis was used to investigate the composition of these nanoparticles. It can be observed in Figure S4 that oleic acid- capped UCNPs exhibit a weight loss during the temperature range of about 200 °C–300 °C, attributing to the loss of oleic acid. However, for the acid-treated bare UCNPs, no weight loss is observed during the temperature range of about 200 °C–300 °C, indicating that oleic acid molecules have been absolutely removed and the UCNPs are bare without attachment. For the PVP-coated UCNPs, a weight loss is observed during the temperature range between 300 °C and 400 °C, corresponding to the loss temperature of PVP. All these results suggest that PVP was successfully functionalized. Then, meso-Tetra(4-carboxyphenyl)porphine (TCPP) and copper ions were utilized as organic linkers and metal centers, respectively to assemble UCNPs/2DMOFs heterostructures. X-ray diffraction (XRD) pattern in Figure 1 b shows that the typical peaks of as-synthesized composite materials are well-matched with the characteristic peaks of UCNPs and Cu-TCPP 2DMOFs, indicating that the composites consist of UCNPs and Cu-TCPP 2DMOFs. As shown in Figure 1 c,d, and Figure S6, the TEM images show that several nanoparticles are well dispersed on the surface of nanosheets, indicating that heterostructures were successfully assembled. More importantly, all the nanoparticles present a plane of the rectangle with a length of about 90 nm and a width of about 60 nm, which corresponds to the lateral surface of UCNPs. The high-resolution TEM image (inset in Figure 1 d) shows that the interplanar spacing of the rectangular plane is 0.32 nm, consistent with that of (100) facet, indicating that the lateral (100) facet of UCNPs directly contacts with 2DMOFs. Furthermore, energy dispersive

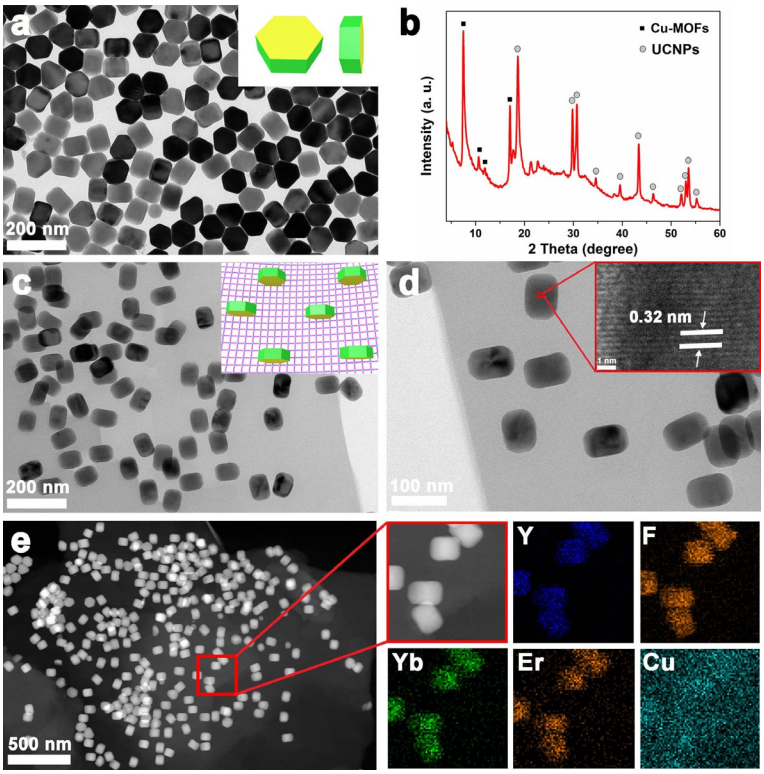

Figure 1. a) TEM image of UCNPs. b) XRD pattern, c,d) TEM images, e) HAADF image and EDS elemental mapping of the as-prepared UCNPs/2DMOFs nanostructures.

X-ray spectroscopy (EDS)-based elemental mapping analysis of the UCNPs/2DMOFs in Figure 1e suggests that the nanoparticles containing Y, F, Yb, and Er were well dispersed on the surface of the Cu-contained 2DMOFs. These findings demonstrate that UCNPs/2DMOFs heterostructures were successfully assembled with facet selectivity.

Scanning electron microscopy (SEM) and atomic force microscopy (AFM) were further performed to characterize the morphology and structures of UCNPs/2DMOFs. As shown in Figure 2a and Figure S6, SEM images indicate that 2DMOFs exhibit thin thickness and UCNPs were well dispersed on the surface of 2DMOFs. The high-resolution SEM image (Figure 2b) also presents that the UCNPs show a uniform shape of a hexagonal prism. More importantly, it can be observed that the lateral surfaces of UCNPs are tightly bound with 2DMOFs while the hexagonal bottom surfaces of UCNPs are perpendicular to the plane of 2DMOFs, indicating that 2DMOFs are assembled with UCNPs at the (100) facets. AFM images further show that UCNPs are assembled onto 2DMOFs with excellent dispersion (Figure 2c,d). Height analysis in Figure 2e suggests that the height of UCNPs is about 90 nm, consistent with the diameter of bottom (001) surface of UCNPs, suggesting that the (001) facet of UCNPs is vertical to 2DMOFs and the (100) facet of UCNPs directly interact with 2DMOFs. These results demonstrate that the assembly of UCNPs and 2DMOFs is highly facet-selective.

The assembly mechanisms of the facet-selective UCNPs/2DMOFs heterostructures were further investigated. Firstly, UCNPs without PVP functionalization and with PVP functionalization were reacted with 2DMOFs precursor solution, respectively, and then the as-obtained materials were characterized by SEM and TEM. As presented in Figure 3a–c, and Figures S7 and S8, when the UCNP was not functionalized with PVP, both the UCNPs and MOFs are separately dispersed without assembly, indicating that PVP plays a necessary role in the facet-selective assembly of UCNPs/2DMOFs. On the contrary, PVP-functionalized UCNPs are well dispersed on the surface of 2DMOFs with high facet selectivity (Figure 3d–f).

Besides, PAA was used as a control molecule to direct the assembly of UCNPs/2DMOFs. Specifically, PAA was functionalized with UCNPs, and then, the PAA-modified UCNPs were assembled with MOFs. As shown in Figure S9, both the (100) and (001) facets of UCNPs can be assembled with 2DMOFs, suggesting that PAA cannot be used to direct the facet-selective assembly of UCNPs/2DMOFs in this condition. The results further demonstrate the unique role of PVP. Furthermore, the assembly process was investigated by characterizing the morphology of formed nanostructures at different reaction times (Figure 3h–k). At the early stage, small 2DMOFs nucleate and grow on the lateral (100) surface of UCNPs and the bottom (001) surface are bare without 2DMOFs assembly.

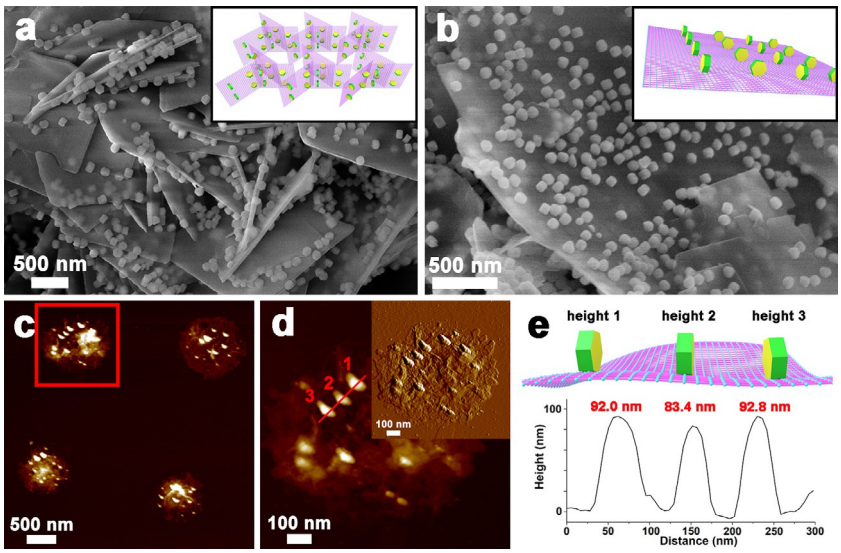

Figure 2. a,b) SEM images of UCNPs/2DMOFs nanostructures. c,d) AFM images of UCNPs/2DMOFs nanostructures. e) Height profiles along the red line in graph (d).

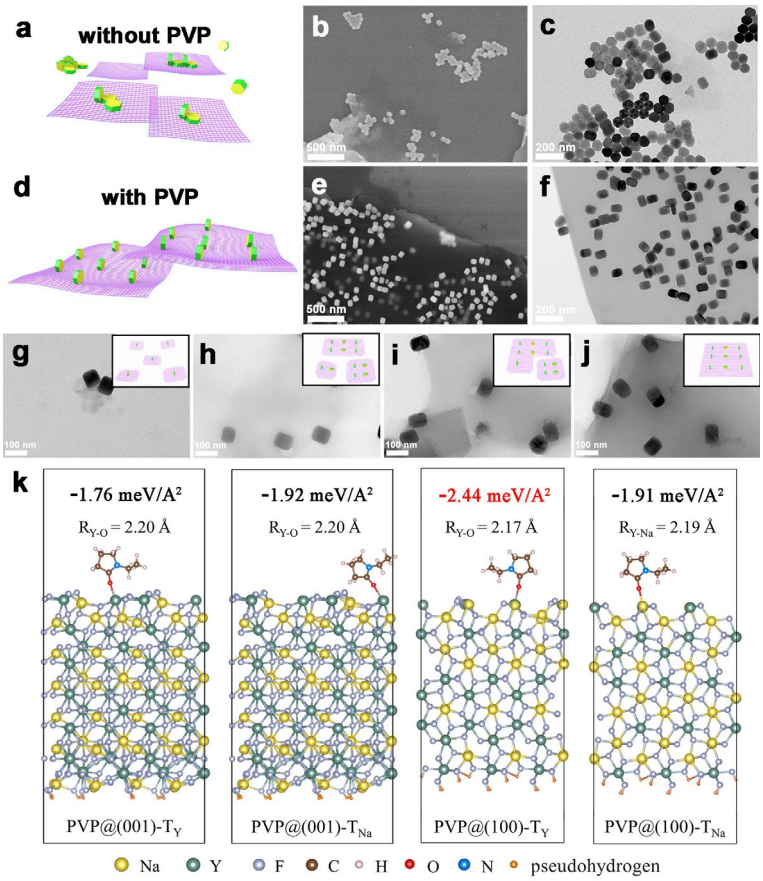

Figure 3. a) Illustration of the as-prepared materials synthesized with bare UCNPs, and the associated b) SEM and c) TEM images. d) Illustration of UCNPs/2DMOFs assembled with PVP-UCNPs, and the associated e) SEM and f) TEM images. g–j) TEM images of UCNPs/2DMOFs formed at different reaction time points: 2 h (g), 4 h (h), 6 h (i), and 10 h (j). k) Simulated calculations of the binding energy of PVP adsorbed onto the (100) and (001) facets of UCNPs.

With the reaction time increasing, 2DMOFs on the lateral (100) facets gradually grow to large size. During the whole process, no 2DMOFs form on the bottom (001) facets of UCNPs. These results indicate that PVP plays essential roles in the facet-selective assembly of UCNPs/2DMOFs. During the whole growth process, MOFs maintains the two-dimensional nanosheets morphology. According to the previous report,[16a] PVP can attached onto the surface of MOFs and direct the anisotropic growth of MOFs, resulting in the formation of 2DMOFs nanosheets. Density functional theory (DFT) was then used to calculate the binding energy of PVP with the different facets of UCNPs (Figure 3g). As is well known, the oxygen atom is considered to be the active site of the PVP molecule. Therefore, we placed a PVP molecule on the bare crystal surface of $NaYF_4$ with O atoms as the active sites. The bond length between the O atom and its nearest Y or Na atom is labeled as $R_{x\text{-}O}$ (x = Y or Na). The initial site of the O atom is above the F (T_F) or Na (T_{Na}) or Y atom (T_Y). The T_F, T_{Na}, and T_{Na} sites are labeled as PVP@(001)-T_F, PVP@(001)-T_{Na}, and PVP@(001)-T_Y in the (001) slab, respectively, and labeled as PVP@(100)-T_F, PVP@(100)-T_{Na}, and PVP@(100)-T_Y in (100) slab, respectively. However, the PVP@(001)-T_F and PVP@(100)-T_F systems are both extremely unstable. The four stable structures are presented in Figure 3g. Surprisingly, the O atom in PVP@(001)-T_{Na} system deviates from the top of Na atom to bond with Y atom after relaxation. The simulated calculation results present that the binding energy of PVP onto the Y atoms in (100) facets exhibit the minimum value (−2.44 meV Å^{-2}), indicating that PVP shows preferential adsorption onto the lateral (100) facets of UCNPs. All the experimental and calculated results suggest that PVP plays an indispensable role in the facet-selective assembly of UCNPs/2DMOFs heterostructures.

Structures of nanomaterials play significant roles in their properties. To investigate the structure–property relationship of facet-selective UCNPs/2DMOFs, the spectroscopic properties of UCNPs/2DMOFs were characterized to investigate the energy transfer between UCNPs and 2DMOFs (Figure 4a). As shown in Figure 4b, the upconversion emission spectrum of UCNPs and the UV/Vis absorption spectrum of UCNPs/2DMOFs show a well-matched spectrum overlapping, demonstrating that the luminescence of UCNPs can be absorbed by the 2DMOFs. Moreover, it can be observed that the emission intensity of UCNPs/2DMOFs is remarkably weaker than that of UCNPs (Figure S10). These results can be explained by the energy transfer between UCNPs and 2DMOFs, contributing to the emission-quenching effect of UCNPs units in UCNPs/2DMOFs. Furthermore, the emission properties of UCNPs/2DMOFs with and without facet selectivity were investigated and compared. It's worth mentioning that the UCNPs/2DMOFs without facet selectivity can be prepared by increasing the content of PVP used to functionalize UCNPs, and TEM and SEM were performed to characterize the morphology of UCNP/2DMOFs without facet selectivity (Figures S11 and S12). As shown in Figure 4c, compared to those without selectivity, facet-selective UCNPs/2DMOFs exhibit a higher emission intensity. It's mainly because for UCNPs/2DMOFs without facet selectivity, 2DMOFs directly interact with both (100) and (001) facets of UCNPs and possess a larger contact area, contributing to the higher energy transfer efficiency. More interestingly, the quantitative analysis of the intensity ratio of green to red (I_{542}/I_{656}) in the inset of Figure 4c presents that facet-selective UCNPs/2DMOFs exhibit a higher I_{542}/I_{656} ratio. This is mainly because 2DMOFs exhibits a higher quenching effect on the green emission than that on the red emission, caused by the higher absorption of 2DMOFs in the green light band. Confocal microscopy images in Figure 4d of UCNPs/2DMOFs with and without facet selectivity also present a similar result, indicating that facet-selective UCNPs/2DMOFs exhibits a higher I_{542}/I_{656} ratio than that without selectivity. All these results demonstrate that UCNPs/2DMOFs with facet selectivity and without selectivity exhibit diverse upconversion emission properties.

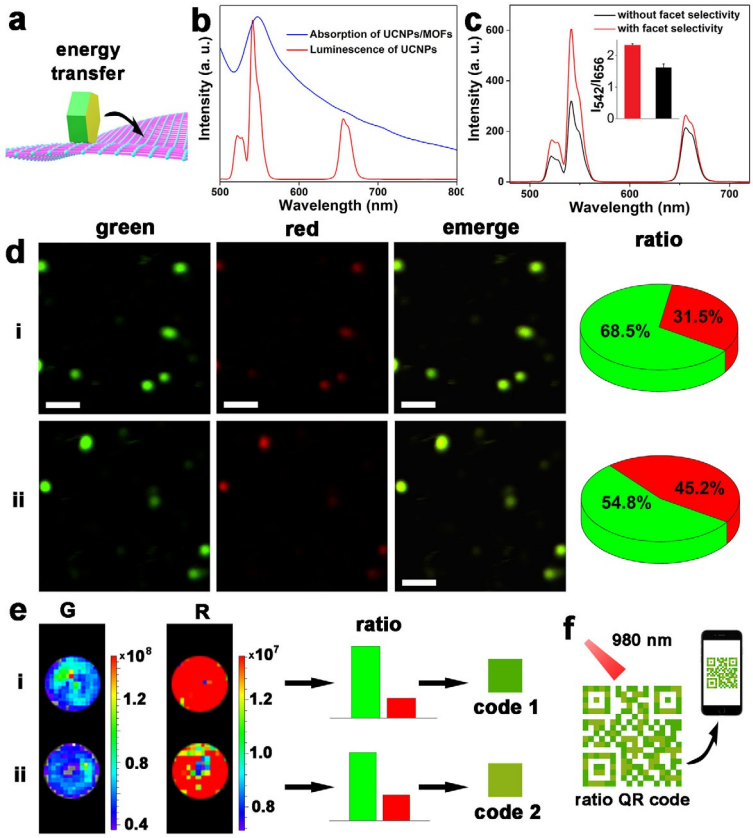

Figure 4. a) Energy transfer between UCNPs and MOFs in the UCNPs/2DMOFs. b) Absorption spectrum of UCNPs/2DMOFs and upconversion luminescence spectrum of UCNPs. c) Upconversion luminescence spectra of UCNPs/2DMOFs with facet selectivity and without selectivity, respectively. Inset: the ratio of the intensity at 542 nm to the intensity at 656 nm. d) Confocal microscopy images of UCNPs/2DMOFs with facet selectivity and without selectivity, respectively. e) Green and red channels in the photographs of upconversion luminescence of UCNPs/2DMOFs and the code principle of UCNPs/2DMOFs. (i) UCNPs/2DMOFs with facet selectivity and (ii) UCNPs/2DMOFs without facet selectivity. f) Illustration of the utilization of a UCNPs/2DMOFs two-dimensional barcode for smartphone applications.

The tunable multicolor emission and the green-to-red ratio of UCNPs/2DMOFs architectures offer a promising strategy for multiplexed coding and anti-counterfeiting. To demonstrate the feasibility of UCNPs/2DMOFs in anticounterfeiting, a coding process based on UCNPs/2DMOFs is illustrated in Figure 4e. Specifically, the green channel photographs and red channel photographs were obtained and the emission intensity was calculated. Then, based on the calculation results, the green-to-red ratios of the UCNPs/2DMOFs with and without facet-selectivity were determined. According to the ratio values, UCNPs/2DMOFs with and without facet-selectivity are defined as code 1 and code 2, respectively. By utilizing the UCNPs/2DMOFs-based codes, a two-dimensional barcode system is expected with both 980 nm excitation and green-to-red ratio as dual codes (Figure S13). Specifically, code 1 and code 2 are randomly placed into different pixels of the two-dimensional barcode, and the pixels unplaced are defined as 0. Without excitation, the patterns can be converted into a black-and-white two-dimensional barcode, in which the pixels placed refer to the black and the pixels unplaced refer to the white. Under the excitation of 980 nm laser, code 1 and code 2 can be recognized with different red-to-green ratios, and the black-and-white two-dimensional barcode can be updated to a ratio two-dimensional barcode. Such a ratio two-dimensional barcode holds great promise in various practical conditions such as on-site payment and authority management (Figure 4f).

Conclusion

In conclusion, the facet-selective binding of PVP to UCNPs enables the synthesis of UCNPs/2DMOFs heterostructures with controlled facet selectivity. UCNPs/2DMOFs exhibit unique optical properties through the energy transfer between two units. To be specific, with more facets of UCNPs involved in the growth of 2DMOFs, the efficiency of energy transfer improves. Such a structure–property relationship establishes a solid foundation for applications in information security. The strategy for the construction of facet-selective UCNPs/2DMOFs heterostructures may open a new door for the design of hierarchical complex nanomaterials and offer a promising strategy to investigate structure–property relationships with potential in biosensing, energy storage and conversion, information technology, and biomedicine.

Acknowledgements

This work was supported by the National Natural Science Foundation of China (21675120, 21904100). Q. Yuan thanks the large-scale instrument and equipment sharing foundation of Wuhan University.

Conflict of Interest

The authors declare no conflict of interest.

Keywords: anti-counterfeiting · facet selectivity · metal–organic frameworks · two dimensional structures · upconversion

[1] a) M. I. Siponen, P. Legrand, M. Widdrat, S. R. Jones, W. J. Zhang, M. C. Chang, D. Faivre, P. Arnoux, D. Pignol, *Nature* **2013**, *502*, 681–684; b) A. Gal, R. Wirth, J. Kopka, P. Fratzl, D. Faivre, A. Scheffel, *Science* **2016**, *353*, 590–593; c) L. M. Gordon, D. Joester, *Nature* **2011**, *469*, 194–197.

[2] a) J. Ren, Y. Wang, Y. Yao, Y. Wang, X. Fei, P. Qi, S. Lin, D. L. Kaplan, M. J. Buehler, S. Ling, *Chem. Rev.* **2019**, *119*, 12279–12336; b) S. Tadepalli, J. M. Slocik, M. K. Gupta, R. R. Naik, S. Singamaneni, *Chem. Rev.* **2017**, *117*, 12705–12763.

[3] a) U. G. Wegst, H. Bai, E. Saiz, A. P. Tomsia, R. O. Ritchie, *Nat. Mater.* **2015**, *14*, 23 – 36; b) Z. Li, H. Liu, R. Wang, C. Ji, Y. Wei, M. Shi, Y. Wang, Y. Du, Y. Zhang, Q. Yuan, C. Yan, *ACS Nano* **2020**, *14*, 16085 – 16095.
[4] a) W. Qin, C. Y. Wang, Y. X. Ma, M. J. Shen, J. Li, K. Jiao, F. R. Tay, L. N. Niu, *Adv. Mater.* **2020**, *32*, 1907833; b) P. Thissen, *Langmuir* **2020**, *36*, 10293 – 10306.
[5] a) J. Meng, S. Wang, *Adv. Funct. Mater.* **2020**, *30*, 1904796; b) S.-Y. Pan, Y.-H. Chen, L.-S. Fan, H. Kim, X. Gao, T.-C. Ling, P.-C. Chiang, S.-L. Pei, G. Gu, *Nat. Sustainability* **2020**, *3*, 399 – 405.
[6] a) A. K. Pearce, T. R. Wilks, M. C. Arno, R. K. O'Reilly, *Nat. Rev. Chem.* **2021**, *5*, 21—45; b) G. L. Koons, M. Diba, A. G. Mikos, *Nat. Rev. Mater.* **2020**, *5*, 584 – 603; c) L. M. Gordon, L. Tran, D. Joester, *ACS Nano* **2012**, *6*, 10667 – 10675.
[7] a) E. Zolotoyabko, *Adv. Mater. Interfaces* **2017**, *4*, 1600189; b) A. Lotsari, A. K. Rajasekharan, M. Halvarsson, M. Andersson, *Nat. Commun.* **2018**, *9*, 4170; c) K. Fukao, T. Nonoyama, R. Kiyama, K. Furusawa, T. Kurokawa, T. Nakajima, J. P. Gong, *ACS Nano* **2017**, *11*, 12103 – 12110.
[8] C. Liu, H. Zhai, Z. Zhang, Y. Li, X. Xu, R. Tang, *ACS Appl. Mater. Interfaces* **2016**, *8*, 29997 – 30004.
[9] Y. Xu, F. Nudelman, E. D. Eren, M. J. M. Wirix, B. Cantaert, W. H. Nijhuis, D. Hermida-Merino, G. Portale, P. H. H. Bomans, C. Ottmann, H. Friedrich, W. Bras, A. Akiva, J. Orgel, F. C. Meldrum, N. Sommerdijk, *Nat. Commun.* **2020**, *11*, 5068.
[10] a) T. J. Kempa, S. K. Kim, R. W. Day, H. G. Park, D. G. Nocera, C. M. Lieber, *J. Am. Chem. Soc.* **2013**, *135*, 18354 – 18357; b) X. J. Wu, J. Chen, C. Tan, Y. Zhu, Y. Han, H. Zhang, *Nat. Chem.* **2016**, *8*, 470 – 475; c) Y. Fu, F. Meng, M. B. Rowley, B. J. Thompson, M. J. Shearer, D. Ma, R. J. Hamers, J. C. Wright, S. Jin, *J. Am. Chem. Soc.* **2015**, *137*, 5810 – 5818.
[11] a) Y. Chong, X. Dai, G. Fang, R. Wu, L. Zhao, X. Ma, X. Tian, S. Lee, C. Zhang, C. Chen, Z. Chai, C. Ge, R. Zhou, *Nat. Commun.* **2018**, *9*, 4861; b) C. Ge, G. Fang, X. Shen, Y. Chong, W. G. Wamer, X. Gao, Z. Chai, C. Chen, J. J. Yin, *ACS Nano* **2016**, *10*, 10436 – 10445.
[12] a) C. Tan, J. Chen, X.-J. Wu, H. Zhang, *Nat. Rev. Mater.* **2018**, *3*, 17089; b) Y. Ge, Z. Huang, C. Ling, B. Chen, G. Liu, M. Zhou, J. Liu, X. Zhang, H. Cheng, G. Liu, Y. Du, C. J. Sun, C. Tan, J. Huang, P. Yin, Z. Fan, Y. Chen, N. Yang, H. Zhang, *J. Am. Chem. Soc.* **2020**, *142*, 18971 – 18980; c) M. Cao, Z. Tang, Q. Liu, Y. Xu, M. Chen, H. Lin, Y. Li, E. Gross, Q. Zhang, *Nano Lett.* **2016**, *16*, 5298 – 5302.
[13] a) Y. Wang, T. Azais, M. Robin, A. Vallee, C. Catania, P. Legriel, G. Pehau-Arnaudet, F. Babonneau, M. M. Giraud-Guille, N. Nassif, *Nat. Mater.* **2012**, *11*, 724 – 733; b) H. E. Lee, H. Y. Ahn, J. Mun, Y. Y. Lee, M. Kim, N. H. Cho, K. Chang, W. S. Kim, J. Rho, K. T. Nam, *Nature* **2018**, *556*, 360 – 365; c) C. Y. Chiu, Y. Li, L. Ruan, X. Ye, C. B. Murray, Y. Huang, *Nat. Chem.* **2011**, *3*, 393 – 399.
[14] a) M. Liu, Z. Li, Y. Li, J. Chen, Q. Yuan, *Chin. Chem. Lett.* **2019**, *30*, 1009 – 1012; b) X. Liu, F. Zhang, X. Jing, M. Pan, P. Liu, W. Li, B. Zhu, J. Li, H. Chen, L. Wang, J. Lin, Y. Liu, D. Zhao, H. Yan, C. Fan, *Nature* **2018**, *559*, 593 – 598.
[15] a) E. Zhu, S. Wang, X. Yan, M. Sobani, L. Ruan, C. Wang, Y. Liu, X. Duan, H. Heinz, Y. Huang, *J. Am. Chem. Soc.* **2019**, *141*, 1498 – 1505; b) S. H. Yoo, T. Eom, S. Kwon, J. Gong, J. Kim, S. J. Cho, R. W. Driver, Y. Lee, H. Kim, H. S. Lee, *J. Am. Chem. Soc.* **2015**, *137*, 2159 – 2162; c) L. L. Li, Y. Lu, *J. Am. Chem. Soc.* **2015**, *137*, 5272 – 5275.
[16] a) M. Zhao, Y. Wang, Q. Ma, Y. Huang, X. Zhang, J. Ping, Z. Zhang, Q. Lu, Y. Yu, H. Xu, Y. Zhao, H. Zhang, *Adv. Mater.* **2015**, *27*, 7372 – 7378; b) F. Cao, M. Zhao, Y. Yu, B. Chen, Y. Huang, J. Yang, X. Cao, Q. Lu, X. Zhang, Z. Zhang, C. Tan, H. Zhang, *J. Am. Chem. Soc.* **2016**, *138*, 6924 – 6927; c) C. Tan, K. Yang, J. Dong, Y. Liu, Y. Liu, J. Jiang, Y. Cui, *J. Am. Chem. Soc.* **2019**, *141*, 17685 – 17695; d) L. Zhuang, L. Ge, H. Liu, Z. Jiang, Y. Jia, Z. Li, D. Yang, R. K. Hocking, M. Li, L. Zhang, X. Wang, X. Yao, Z. Zhu, *Angew. Chem. Int. Ed.* **2019**, *58*, 13565 – 13572; *Angew. Chem.* **2019**, *131*, 13699 – 13706; e) M. Xu, S. Yuan, X. Y. Chen, Y. J. Chang, G. Day, Z. Y. Gu, H. C. Zhou, *J. Am. Chem. Soc.* **2017**, *139*, 8312 – 8319.
[17] a) S. Zhao, Y. Wang, J. Dong, C.-T. He, H. Yin, P. An, K. Zhao, X. Zhang, C. Gao, L. Zhang, J. Lv, J. Wang, J. Zhang, A. M. Khattak, N. A. Khan, Z. Wei, J. Zhang, S. Liu, H. Zhao, Z. Tang, *Nat. Energy* **2016**, *1*, 16184; b) C. Wang, F. Cao, Y. Ruan, X. Jia, W. Zhen, X. Jiang, *Angew. Chem. Int. Ed.* **2019**, *58*, 9846 – 9850; *Angew. Chem.* **2019**, *131*, 9951 – 9955; c) X. Wang, C. Chi, K. Zhang, Y. Qian, K. M. Gupta, Z. Kang, J. Jiang, D. Zhao, *Nat. Commun.* **2017**, *8*, 14460; d) Q. Qian, P. A. Asinger, M. J. Lee, G. Han, K. Mizrahi Rodriguez, S. Lin, F. M. Benedetti, A. X. Wu, W. S. Chi, Z. P. Smith, *Chem. Rev.* **2020**, *120*, 8161 – 8266; e) A. Hu, Q. Pang, C. Tang, J. Bao, H. Liu, K. Ba, S. Xie, J. Chen, J. Chen, Y. Yue, Y. Tang, Q. Li, Z. Sun, *J. Am. Chem. Soc.* **2019**, *141*, 11322 – 11327; f) M. Zhao, Q. Lu, Q. Ma, H. Zhang, *Small Methods* **2017**, *1*, 1600030.
[18] a) J. Zhou, Q. Liu, W. Feng, Y. Sun, F. Li, *Chem. Rev.* **2015**, *115*, 395 – 465; b) G. Chen, H. Qiu, P. N. Prasad, X. Chen, *Chem. Rev.* **2014**, *114*, 5161 – 5214; c) B. Zhou, B. Shi, D. Jin, X. Liu, *Nat. Nanotechnol.* **2015**, *10*, 924 – 936; d) Z. Yuan, L. Zhang, S. Li, W. Zhang, M. Lu, Y. Pan, X. Xie, L. Huang, W. Huang, *J. Am. Chem. Soc.* **2018**, *140*, 15507 – 15515; e) J. Zhao, H. Chu, Y. Zhao, Y. Lu, L. Li, *J. Am. Chem. Soc.* **2019**, *141*, 7056 – 7062.
[19] a) Y. Li, Z. Di, J. Gao, P. Cheng, C. Di, G. Zhang, B. Liu, X. Shi, L. D. Sun, L. Li, C. H. Yan, *J. Am. Chem. Soc.* **2017**, *139*, 13804 – 13810; b) X. Liu, Y. Wang, X. Li, Z. Yi, R. Deng, L. Liang, X. Xie, D. T. B. Loong, S. Song, D. Fan, A. H. All, H. Zhang, L. Huang, X. Liu, *Nat. Commun.* **2017**, *8*, 899; c) D. Li, S. H. Yu, H. L. Jiang, *Adv. Mater.* **2018**, *30*, 1707377; d) M. Tang, X. Zhu, Y. Zhang, Z. Zhang, Z. Zhang, Q. Mei, J. Zhang, M. Wu, J. Liu, Y. Zhang, *ACS Nano* **2019**, *13*, 10405 – 10418; e) S. Wen, J. Zhou, P. J. Schuck, Y. D. Suh, T. W. Schmidt, D. Jin, *Nat. Photonics* **2019**, *13*, 828 – 838.
[20] D. Liu, X. Xu, Y. Du, X. Qin, Y. Zhang, C. Ma, S. Wen, W. Ren, E. M. Goldys, J. A. Piper, S. Dou, X. Liu, D. Jin, *Nat. Commun.* **2016**, *7*, 10254.
[21] Z. Li, Y. Zhang, *Nanotechnology* **2008**, *19*, 345606.

Manuscript received: March 10, 2021
Accepted manuscript online: May 28, 2021
Version of record online: June 30, 2021

